Acetylene Gas-Sensing Properties of Layer-by-Layer Self-Assembled Ag-Decorated Tin Dioxide/Graphene Nanocomposite Film

Chuanxing Jiang [1], Dongzhi Zhang [1],* ID **, Nailiang Yin [1], Yao Yao [2], Talgar Shaymurat [3] and Xiaoyan Zhou [4]**

[1] College of Information and Control Engineering, China University of Petroleum (East China), Qingdao 266580, China; jiangchuanxing@126.com (C.J.); nailiang_yin@163.com (N.Y.)
[2] College of Communication Engineering, Chengdu University of Information Technology, Chengdu 610225, China; yaoyao@cuit.edu.cn
[3] Key Laboratory of New Energy and Materials Research, Xinjiang Institute of Engineering, Urumqi 83000, China; talgar.shaymurat@vip.163.com
[4] College of Science, China University of Petroleum (East China), Qingdao 266580, China; zhouxiaoyan@upc.edu.cn
* Correspondence: dzzhang@upc.edu.cn; Tel.: +86-532-86981335

Abstract: This paper demonstrates an acetylene gas sensor based on an Ag-decorated tin dioxide/reduced graphene oxide ($Ag–SnO_2/rGO$) nanocomposite film, prepared by layer-by-layer (LbL) self-assembly technology. The as-prepared $Ag–SnO_2/rGO$ nanocomposite was characterized by scanning electron microscopy (SEM), transmission electron microscopy (TEM), X-ray diffraction (XRD) and Raman spectrum. The acetylene sensing properties were investigated using different working temperatures and gas concentrations. An optimal temperature of 90 °C was determined, and the $Ag–SnO_2/rGO$ nanocomposite sensor exhibited excellent sensing behaviors towards acetylene, in terms of response, repeatability, stability and response/recovery characteristics, which were superior to the pure SnO_2 and SnO_2/rGO film sensors. The sensing mechanism of the $Ag–SnO_2/rGO$ sensor was attributed to the synergistic effect of the ternary nanomaterials, and the heterojunctions created at the interfaces between SnO_2 and rGO. This work indicates that the $Ag–SnO_2/rGO$ nanocomposite is a good candidate for constructing a low-temperature acetylene sensor.

Keywords: graphene; layer-by-layer self-assembly; nanocomposite film; acetylene sensor

1. Introduction

Acetylene (C_2H_2) is a colorless and highly combustible gaseous hydrocarbon, widely used as a fuel in many industrial fields, such as metal welding [1], polyacetylene preparation [2], lithium-ion batteries [3], and conductive plastic manufacturing [4]. However, acetylene is unstable and there is a huge potential risk of fire or explosive accidents during its compression and heat treatment, or due to leakage. Furthermore, the dissolved content of acetylene gas in power transformer oil is critical to the safety and reliability of the transformer system [5,6]. Therefore, reliable, economical and portable acetylene gas sensors are of great importance to many applications. In recent years, a lot of interest has been attracted surrounding the development of effective techniques and sensitive methods for acetylene gas detection, such as photoacoustic spectroscopy [7], optical fiber [6,8] and metal-oxide semiconductors (MOS) and nanomaterial-based sensors (i.e., PdO-decorated SnO_2 [9], Au/multi-wall carbon nanotubes [10], Sm_2O_3-decorated SnO_2 [11], Ag-loaded ZnO [12–14] and NiO/SnO_2 heterostructures [15]). Among them, metal oxides have become important candidates

for acetylene sensing due to their unique advantages—such as their small size and simplicity of integration—but they lack selectivity towards different gas species, and often require high operating temperatures and have high power consumption [16–20].

The state-of-the-art MOS-based acetylene sensor focuses on noble metal-metal oxide nanohybrids and heterometal oxide nanostructures. Zhang et al. reported on the hydrothermal synthesis of hierarchical nanoparticle-decorated ZnO microdisks for acetylene gas sensing at 420 °C [21]. Tamaekong et al. synthesized Pt/ZnO thick film, using the flame spray pyrolysis (FSP) technique, and a low detection limit for 50 ppm acetylene gas was obtained at an operating temperature of 300 °C [22]. Chen et al. synthesized Pd-doped SnO_2 nanoparticles using a hydrothermal method for detecting acetylene gas dissolved in power transformer oil, indicating a sensor response of 7.22 for 100 ppm acetylene at 350 °C [23]. Zhou et al. fabricated a planar-type acetylene gas sensor based on Sm_2O_3-decorated SnO_2 heterostructures, and showed that the optimum operating temperature of the sensor for 50 ppm of acetylene is 260 °C [11]. Uddin et al. developed a novel flexible acetylene gas sensor, consisting of Ag-loaded vertical ZnO nanorods, supported by a polyimide/ polytetrafluoroethylene (PI/PTFE) substrate, using a hydrothermal-radio frequency (RF) magnetron sputtering method and showed that its best sensing performance was at 200 °C [12]. As a two-dimensional nanomaterial, graphene has attracted much attention since its discovery, because of its excellent characteristics, such as its electrical, chemical and optical properties [24,25]. Graphene-based nanocomposites have been widely used in membrane science and technology [26,27]. Uddin et al. synthesized a ZnO/reduced graphene oxide (rGO) composite using a solvothermal method, which exhibited preferential detection of acetylene gas with good selectivity, long-term stability, and fast response/recovery times at 250 °C [28]. The presented progresses suggest that noble metal doping and graphene addition techniques are effective for lowering the operating temperature and improving the acetylene sensing performance of MOS-based sensors.

In this work, we fabricated a low-temperature acetylene gas sensor based on a layer-by-layer, self-assembled $Ag–SnO_2$/rGO ternary nanocomposite film, for the first time. The as-prepared nanocomposite was characterized by scanning electron microscopy (SEM), transmission electron microscopy (TEM), X-ray diffraction (XRD) and Raman spectrum, which confirmed its successful formation and rationality. The acetylene sensing properties were investigated under different working temperatures and gas concentrations. An optimal temperature of 90 °C was determined, and the $Ag–SnO_2$/rGO nanocomposite sensor exhibited excellent sensing behaviors towards acetylene in terms of response, repeatability, stability and response/recovery characteristics. The underlying sensing mechanism of the $Ag–SnO_2$/rGO sensor was further discussed.

2. Materials and Methods

2.1. Materials

The high-purity graphene oxide (GO) nanosheets (>99%) were supplied by Chengdu Organic Chemicals Co. Ltd. (Chengdu, China). The GO used was graphene nanosheet, negatively decorated with oxygen functional groups and carboxylic groups, which were located at the sheet surface. The GO suspension was 0.25 wt % concentrated at pH 4.5. Tin chloride pentahydrate ($SnCl_4·5H_2O$) and hydrazine hydrate were obtained from Sinopharm Chemical Reagent Co. Ltd. (Shanghai, China). Polyelectrolytes used for layer-by-layer (LbL) assembly were 1.5 wt % poly(diallyldimethylammonium chloride) [PDDA (Sigma-Aldrich Co., Saint Louis, MO, USA), molecular weights (MW) of 200–350 K] and 0.3 wt % poly(sodium 4-styrenesulfonate) [PSS (Sigma-Aldrich Co., Saint Louis, MO, USA), MW of 70 K] with 0.5 M NaCl (West Long Chemical Co., Ltd., Guangdong, China) in both, to provide better surface coverage. All reagents were used without further purification.

2.2. Preparation of the Ag–SnO2/rGO Nanocomposite

Figure 1a illustrates the hydrothermal synthesis of SnO_2. Firstly, 24 mg of $SnCl_4 \cdot 5H_2O$ was dissolved in 30 mL of deionized water and stirred for 1 h. After that, the solution was hydrothermally treated at 120 °C for 12 h, and then washed with deionized water and ethanol several times. The SnO_2 aqueous solution was obtained after being ultrasonicated for 1 h and centrifugated for 15 min. A substrate with interdigitated electrodes for resistive sensing and heating elements was fabricated. The Ag–SnO_2/rGO nanocomposite was deposited on the sensing electrodes using the layer-by-layer (LbL) self-assembly technique, which is shown in Figure 1b. Two bi-layers of PDDA/PSS were firstly self-assembled as the precursor layer, followed by alternative immersion into SnO_2, GO, SnO_2 and Ag suspensions. The immersing time here used was 10 min for the polyelectrolytes and 15 min for the SnO_2, GO and Ag suspensions. Intermediate rinsing with deionized water and drying with nitrogen gas were required after each monolayer assembly, to reinforce the interconnection between the layers. The film was formed due to the interaction of electrostatic forces between the positively and negatively charged nanoparticles. The first SnO_2 layer (positively charged) was designed for the intermediate bonding between PSS (negatively charged) and GO (negatively charged). The Ag–SnO_2/rGO nanocomposite sensor was obtained via the thermal reduction of GO into rGO at 220 °C for 5 h in an oven. Furthermore, the pure SnO_2 and SnO_2/rGO film sensor were fabricated to allow a comparison between the drop-casting and LbL self-assembly methods, respectively.
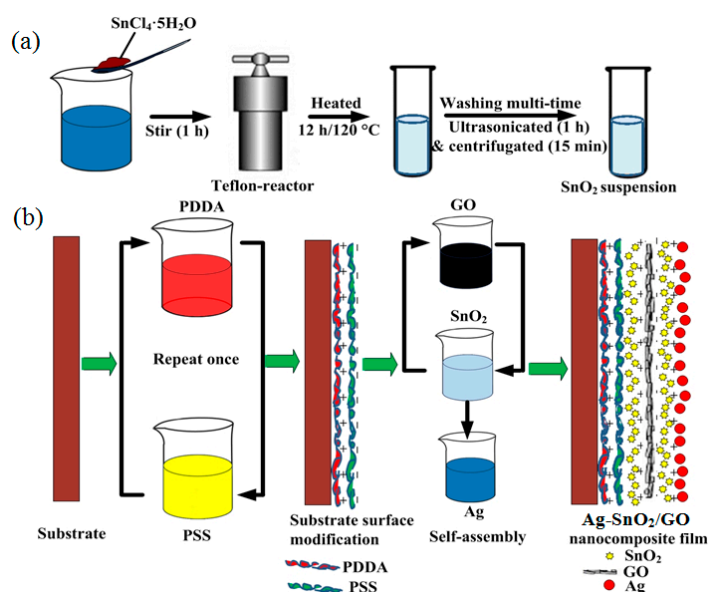

Figure 1. (**a**) Hydrothermal synthesis of SnO_2 and (**b**) layer-by-layer self-assembly of the Ag–SnO_2/GO nanocomposite film.

2.3. Instruments and Analysis

Surface microscopy of the Ag–SnO_2/rGO sample was carried out with a scanning electron microscope (SEM, Hitachi S-4800, Tokyo, Japan). The X-ray diffraction (XRD) spectrum of the samples was examined with an X-ray diffractometer (Rigaku D/Max 2500PC, Tokyo, Japan) using Cu Kα radiation with a wavelength of 1.5418 Å. The lattice fringes of Ag–SnO_2/rGO were inspected with a transmission electron microscope (FEI Tecnai G2 F20, Shanghai, China). The nanostructural and compositional features of the Ag–SnO_2/rGO and SnO_2/rGO samples were characterized by Raman spectra (RamLab-010, Horiba Jobin Yvon, Paris, France).

A schematic of the experimental setup for acetylene sensing is shown in Figure 2. The acetylene gas sensing properties were investigated by exposing the sensor to various concentrations of acetylene gas, and the desired gas concentration was obtained by injecting the required quantity of acetylene

into a sealed chamber using a syringe. The working temperature for the sensor was adjusted through applying varying voltages to the heating electrodes with a power source (Gwinstek GPD-4303S, New Taipei, Taiwan). The heater resistor (R_H), heating voltage (V_H), sensor resistance (R_S) and protection resistor (R_L) made up the simplified circuit. The sensor resistance was recorded using a data logger (Agilent 34970A, San Jose, CA, USA), connected to a computer via a recommended standard (RS)-232 interface. The sensitivity of the sensor was defined as $S = (R_0 - R_g)/R_0 \times 100\%$, where R_0 and R_g were the sensor resistances in dry air and acetylene gas, respectively. The time taken by a sensor to achieve 90% of the total resistance change was defined as the response or recovery time.
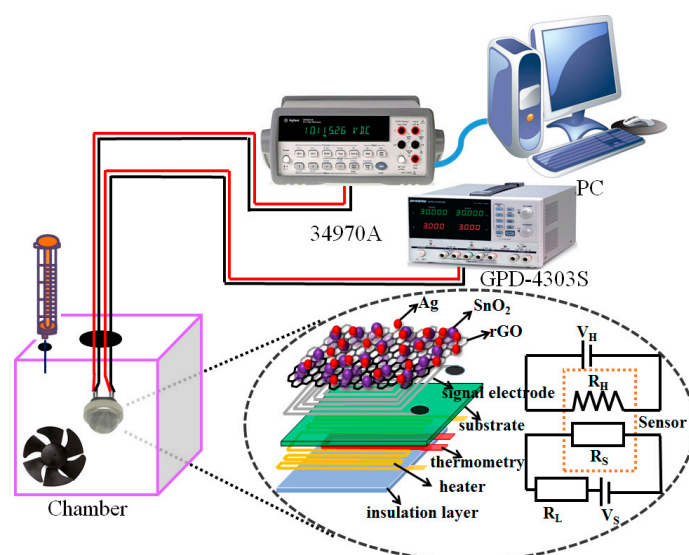

Figure 2. Schematic of the acetylene sensing experimental setup.

3. Results and Discussion

3.1. Sample Characterization

Figure 3a shows the SEM image of the Ag–SnO$_2$/rGO nanocomposite film. SnO$_2$ microspheres and Ag nanoparticles (NPs) attached to the surface of rGO sheets are clearly observed. Figure 3b shows a high-resolution TEM image of the Ag–SnO$_2$/rGO nanocomposite, and lattice fringe spacings of 0.35, 0.33 and 0.23 nm for rGO, SnO$_2$ and Ag, respectively, are measured. Figure 3c indicates the XRD spectrum for the GO, rGO, SnO$_2$ and Ag–SnO$_2$/rGO nanocomposite films. Obvious peaks at 2θ angles of 10.78° and 24.7° are observed for the GO and thermally treated rGO, respectively, which is in agreement with previously published results, and further confirms the successful reduction of GO via thermal treatment [29–31]. The XRD spectrum of SnO$_2$ indicates several peaks at 26.41°, 33.82°, 37.60°, 51.73° and 65.68°, indexed to the (110), (101), (200), (211) and (301) planes of rutile SnO$_2$, which is in accordance with the data from JCPDS Card no. 41-1445 [32], and confirms the successful formation of SnO$_2$ nanocrystals. Apart from the characteristic peaks attributed to SnO$_2$, the XRD spectrum of the Ag–SnO$_2$/rGO nanocomposite exhibited distinct peaks at 38.10°, 44.37° and 64.17°, which indexed to the (111), (200) and (220) planes of Ag crystallines, respectively [33]. However, the broad peak of rGO is not obvious in the XRD pattern of the Ag–SnO$_2$/rGO nanocomposite, probably because the weak peak of rGO is swamped by the high intensity peak of the SnO$_2$ at the 2θ angle of 26.41° [34,35]. Figure 3d shows the Raman spectrum of the SnO$_2$/rGO and Ag–SnO$_2$/rGO nanocomposites. The peaks located at 633 cm^{-1} in the SnO$_2$/rGO and Ag–SnO$_2$/rGO nanocomposites are typical Raman peaks of SnO$_2$. The weak peaks located at 796 and 1588 cm^{-1} for the two samples are attributed to the Ag NPs. The peaks located at 1363 and 1640 cm^{-1} are attributed to defects and disorder in the graphite layer.
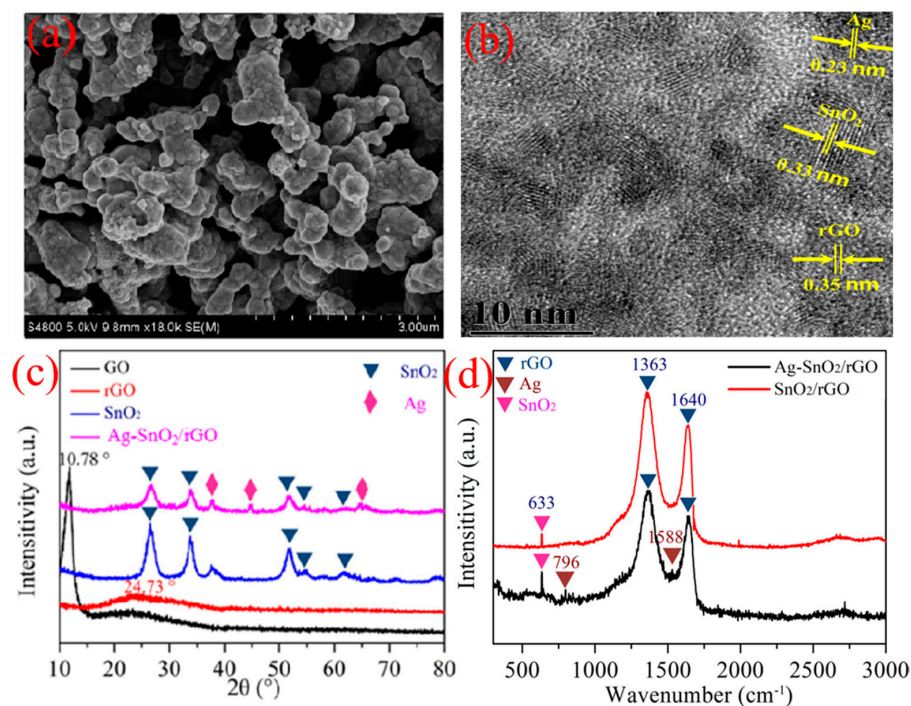
Figure 3. (**a**) SEM characterization of the Ag–SnO$_2$/rGO nanocomposite, (**b**) TEM image of the Ag–SnO$_2$/rGO nanocomposite, (**c**) XRD spectrum of GO, rGO, SnO$_2$ and the Ag–SnO$_2$/rGO nanocomposite, (**d**) Raman spectrum of the SnO$_2$/rGO and Ag–SnO$_2$/rGO nanocomposites.

3.2. Acetylene Sensing Properties

Figure 4 shows the sensitivity of the Ag–SnO$_2$/rGO nanocomposite sensor to 100 ppm acetylene under operating temperatures of 25 to 170 °C. The sensor sensitivity increases and reaches its highest value at 90 °C, and then decreases with any further increase in temperature. This can be explained by the fact that the appropriate operating temperature improves sensor sensitivity, but higher temperatures lower the binding energies of gas molecules and sensing film. An optimal temperature of 90 °C was determined. Therefore, the operating temperature of 90 °C was selected for the sensor in the following experiments.
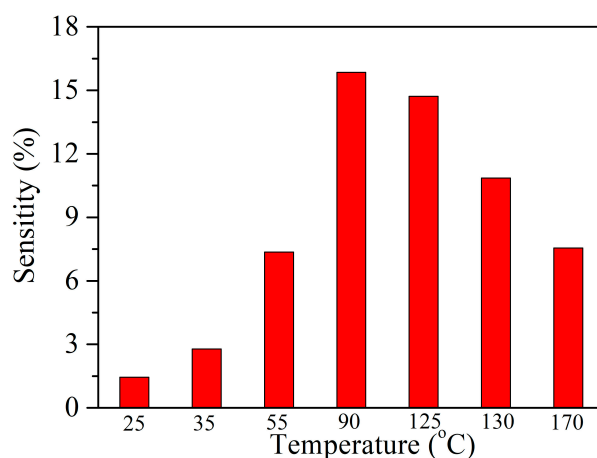

Figure 4. The sensitivity of the Ag–SnO$_2$/rGO nanocomposite sensor to 100 ppm acetylene under different operating temperatures.

Figure 5 shows the sensitivity of pure SnO_2, SnO_2/rGO and Ag–SnO_2/rGO film sensors to 50 ppm acetylene at 90 °C. We found that the Ag–SnO_2/rGO film sensor yielded the highest sensitivity among the three sensors. Moreover, the Ag–SnO_2/rGO film sensor showed a shorter response/recovery time than the other two sensors. A response time and recovery time of 235 and 160 s, respectively, were observed for the Ag–SnO_2/rGO film sensor upon exposure to 50 ppm acetylene.
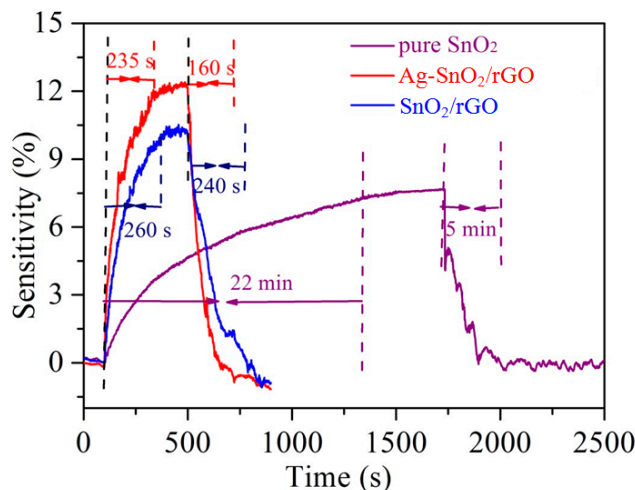

Figure 5. The sensitivity of pure SnO_2, SnO_2/rGO and Ag–SnO_2/rGO film sensors to 50 ppm acetylene at 90 °C.

Figure 6 shows the resistance measurements for the Ag–SnO_2/rGO nanocomposite film sensor upon exposure to acetylene gas, of cumulative concentrations, at 90 °C. The test was performed by exposing the sensor to 5, 10, 50, 100, 150 and 500 ppm of acetylene. The resistance of the Ag–SnO_2/rGO nanocomposite sensor decreased with increasing concentrations of acetylene, indicating the n-type semiconductor-like behavior of Ag–SnO_2/rGO to acetylene (reducing gas). The inset of Figure 6 plots the fitted function of sensor sensitivity (Y) and acetylene concentration (X) as $Y = 32.09 - 25.42e^{-X/236.4}$.
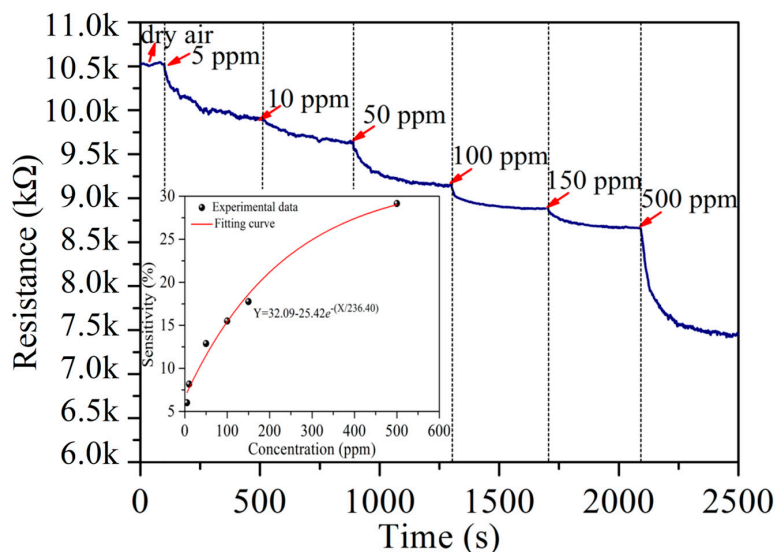

Figure 6. Resistance measurement of the Ag–SnO_2/rGO nanocomposite film sensor upon exposure to acetylene gas with cumulated concentrations at 90 °C.

Figure 7 shows the repeatability of the Ag–SnO$_2$/rGO film sensor with concentrations of 5, 150 and 500 ppm acetylene at 90 °C. There were no significant changes in sensor sensitivity during the repeated exposure/recovery cycles, indicating an acceptable repeatability for acetylene sensing. Figure 8 demonstrates the typical response and recovery curves of the Ag–SnO$_2$/rGO film sensor towards an acetylene pulse, at concentrations between 0 and 500 ppm, exhibiting good response/recovery behavior.
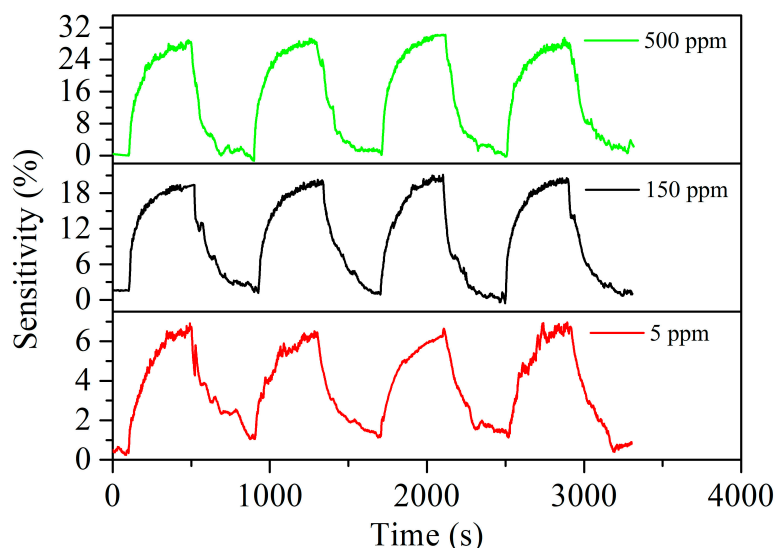

Figure 7. Repeatability of the Ag–SnO$_2$/rGO nanocomposite film sensor toward acetylene concentrations of 5, 150 and 500 ppm at 90 °C.
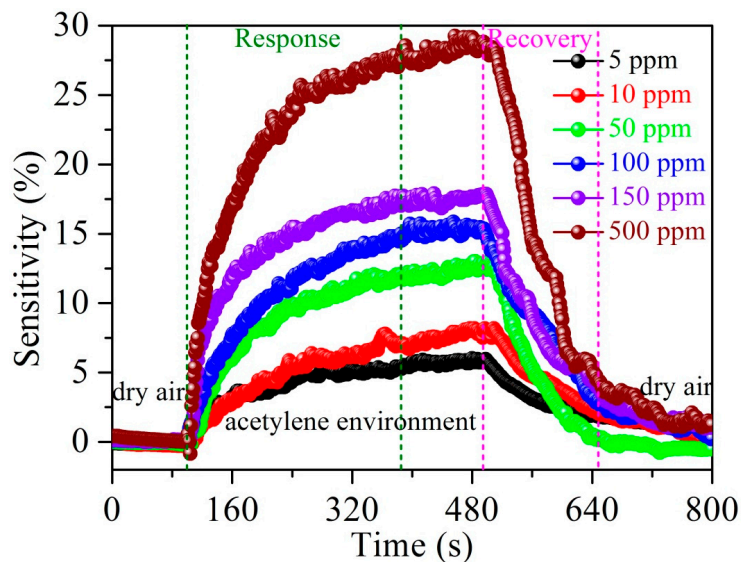

Figure 8. Typical response and recovery curves of the Ag–SnO$_2$/rGO nanocomposite film sensor to acetylene pulses between 0 and 500 ppm.

Figure 9 shows the response of the Ag–SnO$_2$/rGO nanocomposite film sensor to concentrations of 5, 150, and 500 ppm acetylene gas, measured every five days for over 30 days. It was clearly shown that the sensor response does not vary significantly with time, confirming that the Ag–SnO$_2$/rGO nanocomposite film sensor has good long-term stability. Figure 10 shows the experimental current–voltage (I–V) curves for the SnO$_2$, SnO$_2$/rGO and Ag–SnO$_2$/rGO film devices, measured by applying voltages from −4 to 4 V. It is clearly shown that the measurement results indicate good Ohmic contact to n-type

semiconductors for the three devices. A larger current passes through the Ag–SnO$_2$/rGO sensor than that of the SnO$_2$/rGO and SnO$_2$ sensors. This is because the doping of Ag and rGO results in a decrease in the resistance of the Ag–SnO$_2$/rGO film. Table 1 presents the performance of the proposed acetylene gas sensor in comparison with previous reported works [12,13,15,23,36–38]. The working temperature and responses for the prepared sensor are comparable to metal oxide-based sensors made by hydrothermal-RF magnetron sputtering, hydrothermal, electrospinning, spin-coating and sol-gel methods. The presented Ag–SnO$_2$/rGO film sensor exhibited a much higher response and a lower working temperature than that of its MOS-based counterparts.
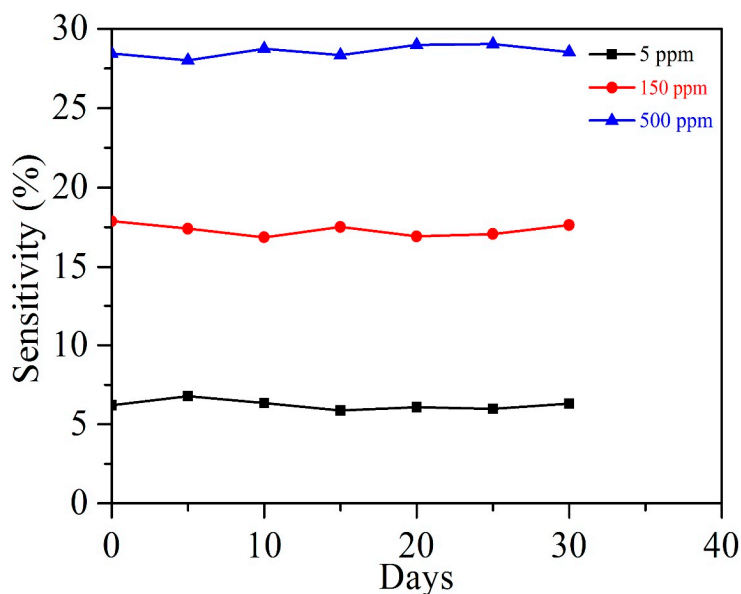

Figure 9. Long-term stability of the Ag–SnO$_2$/rGO nanocomposite film sensor, measured every five days for over 30 days.
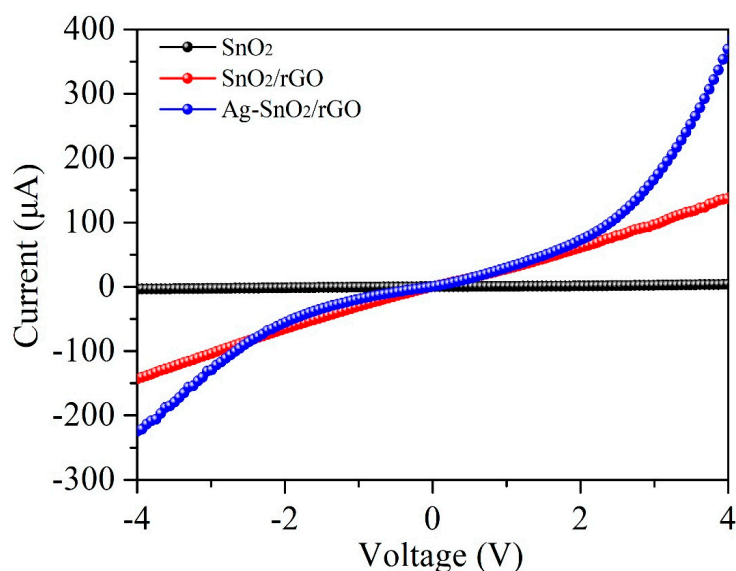

Figure 10. The measured I–V curves of the SnO$_2$, SnO$_2$/rGO and Ag–SnO$_2$/rGO films.

Table 1. Performance of the presented sensor in this work compared with previous works.

Sensing Material	Fabrication Method	Work Temperature	Response	Reference
Ag–SnO$_2$/rGO	Layer-by-layer self-assembly	90 °C	15.8 @100 ppm	This paper
Ag–ZnO nanorods	Hydrothermal-radio frequency (RF) magnetron sputtering	200 °C	27.2 @1000 ppm	[12]
Ag-hierarchical ZnO	Hydrothermal method	200 °C	1.92 @1000 ppm	[13]
NiO/SnO$_2$	Hydrothermal method	206 °C	13.8 @100 ppm	[15]
PdO-SnO$_2$	Hydrothermal method	350 °C	7.22 @100 ppm	[23]
Ni-ZnO	Electrospinning method	250 °C	17 @2000 ppm	[36]
SnO$_2$	Spin-coating method	300 °C	6.3 @10000 ppm	[37]
Sm$_2$O$_3$/SnO$_2$	Sol-gel method	180 °C	63.8 @1000 ppm	[38]

3.3. Acetylene-Sensing Mechanism

The Ag–SnO$_2$/rGO ternary nanocomposite film demonstrated excellent sensing properties towards acetylene gas at low temperatures. Its sensitive mechanism can be attributed to the synergistic effect of the ternary hybrids and the created potential barrier. Pristine SnO$_2$ is an n-type semiconductor and electrons are majority carriers. Graphene, as one of the emerging 2D nanomaterials, has a unique layered structure, a large surface area-to-volume ratio and excellent electrical properties, which greatly facilitate the absorption and diffusion of acetylene gas molecules. Figure 11 shows the sensing mechanism of the Ag–SnO$_2$/rGO nanocomposite film in air and acetylene gas. The oxygen molecules adsorbed on the conduction band of n-type SnO$_2$ are ionized to oxygen negative ions through the trapping of free electrons from the surface of the SnO$_2$ [39]. When the sensor is exposed to acetylene gas, the adsorbed acetylene interacts with the oxygen's negative ions and produces carbon dioxide, water molecules and free electrons. The reaction is expressed as C_2H_2 (ads) + O^- (ads) $\rightarrow CO_2 + H_2O + e^-$, which leads to a decrease in the sensor's resistance [14,28].
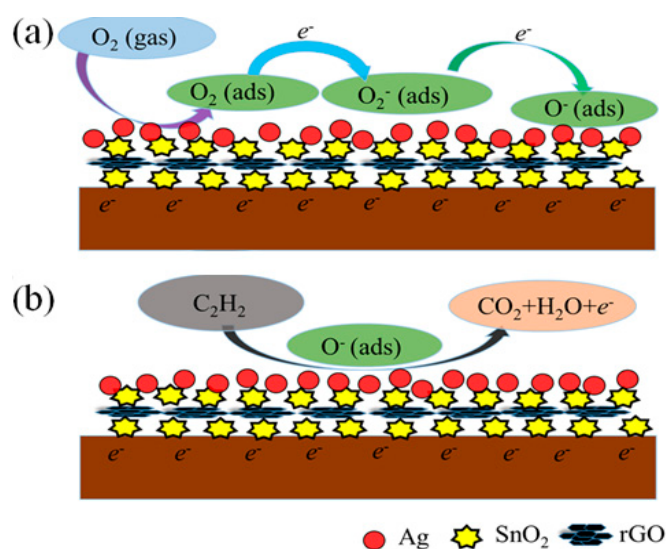

Figure 11. The sensing mechanism of the Ag–SnO$_2$/rGO nanocomposite film in (**a**) air and (**b**) acetylene gas.

The formation of a heterojunction at the interface between rGO and SnO$_2$ is beneficial, because it enhances the acetylene-sensing properties. Figure 12a shows a schematic of an energy band diagram of the SnO$_2$/rGO heterojunction. The band-gaps for n-type SnO$_2$ and p-type rGO are 3.6 and 0.4 eV, respectively [34] and their work functions are 4.5 and 5.1 eV for SnO$_2$ and rGO, respectively [40,41]. Because the Fermi energies are not at the same level and the rGO has a higher work function, when SnO$_2$ and rGO come into contact with each other, electrons transfer from SnO$_2$ to rGO, and holes flow in the opposite direction until a dynamic equilibrium state is reached, and thus a depletion layer is formed at the interface [42]. Figure 12b shows the variation of depletion layer thickness

for the SnO_2/rGO heterojunction. When the sensor was exposed to acetylene gas, the interaction between adsorbed O^- and acetylene molecules released free electrons, with the released free electrons increasing the n-type doping of SnO_2. Higher SnO_2 doping results in a reduced depletion layer in SnO_2, thereby decreasing the sensor resistance during acetylene gas exposure.
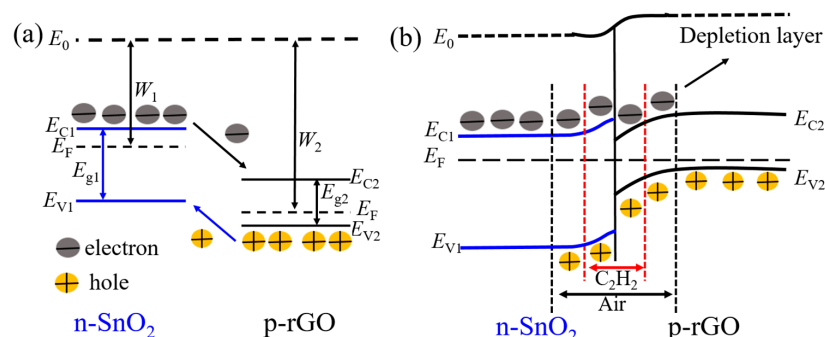

Figure 12. Schematic of the energy band diagram and the variation in depletion layer thickness for the SnO_2/rGO heterojunction. (E_C, conductor band; E_g, band gap; E_V, valence band; E_F, Fermi level; W, work function)

The Ag NPs in the nanocomposite have a positive effect on electronic sensitization during gas adsorption [43,44]. A potential barrier can be created at the contact interface between SnO_2 and Ag, which is beneficial to the enhancement of gas-sensing. Electrons transfer from SnO_2 to Ag NPs and form a highly-resistive "barrier layer" in air, and Ag NPs become centers for electron accumulation. When the sensor is exposed to acetylene gas, electrons transfer from acetylene gas to the Ag NPs and then to SnO_2; the highly-resistive "barrier layer" is transformed into a highly-conductive "anti-barrier layer", which improves the electron mobility and sensing performance of the Ag–SnO_2/rGO nanocomposite sensor.

4. Conclusions

In this work, an acetylene gas sensor, based on Ag–SnO_2/rGO nanocomposite film was fabricated by layer-by-layer self-assembly technology. Successful preparation of the Ag–SnO_2/rGO nanocomposite was characterized and confirmed by means of SEM, TEM, XRD and Raman spectrum. The Ag–SnO_2/rGO nanocomposite sensor exhibited excellent sensing behaviors towards acetylene in terms of response, repeatability, stability and response/recovery characteristics at an optimal temperature of 90 °C, which are superior to pure SnO_2 and SnO_2/rGO film sensors. The underlying sensing mechanism of the Ag–SnO_2/rGO sensor was explored. This work provides guidance for an acetylene sensor based on Ag–SnO_2/rGO ternary nanocomposites.

Author Contributions: Dongzhi Zhang supervised this work and wrote the article; Chuanxing Jiang and Nailiang Yin performed the experiment and analyzed the data; Yao Yao, Talgar Shaymurat and Xiaoyan Zhou analyzed part of the sensing mechanism.

Conflicts of Interest: The authors declared that they have no conflict of interest to this work.

References

1. Antonsson, A.-B.; Christensson, B.; Berge, J.; Sjögren, B. Fatal carbon monoxide intoxication after acetylene gas welding of pipes. *Ann. Occup. Hyg.* **2013**, *57*, 662–666. [PubMed]

2. Steinmetz, J.; Lee, H.-J.; Kwon, S.; Lee, D.-S.; Goze-Bac, C.; Abou-Hamad, E.; Kim, H.; Park, Y.W. Routes to the synthesis of carbon nanotube-polyacetylene composites by Ziegler-Natta polymerization of acetylene inside carbon nanotubes. *Curr. Appl. Phys.* **2007**, *7*, 39–41. [CrossRef]

3. Saroha, R.; Panwar, A.K. Effect of in situ pyrolysis of acetylene (C_2H_2) gas as a carbon source on the electrochemical performance of $LiFePO_4$ for rechargeable lithium-ion batteries. *J. Phys. D Appl. Phys.* **2017**, *50*, 255501. [CrossRef]

4. Bastos, D.C.; Dos Santos, A.E.F.; Simao, R.A. Acetylene coating on cornstarch plastics produced by cold plasma technology. *Starch-Stärke* **2014**, *66*, 267–273. [CrossRef]

5. Jin, L.; Chen, W.; Zhang, H.; Xiao, G.; Yu, C.; Zhou, Q. Characterization of reduced greaphene oxide (rGO)-loaded SnO_2 nanocomposite and applications in C_2H_2 gas detection. *Appl. Sci.* **2017**, *7*, 19. [CrossRef]

6. Wan, F.; Zhou, Q.; Zou, J.; Gu, Z.; Chen, W.; Wang, C. Using a sensitive optical system to analyze gases dissolved in samples extracted from transformer oil. *IEEE Electr. Insul. Mag.* **2014**, *30*, 15–22. [CrossRef]

7. Chen, W.; Liu, B.; Zhou, H.; Wang, Y.; Wang, C. Diode laser-based photoacoustic spectroscopy detection of acetylene gas and its quantitative analysis. *Eur. Trans. Electr. Power* **2012**, *22*, 226–234. [CrossRef]

8. Yan, G.; Zhang, A.P.; Ma, G.; Wang, B.; Kim, B.; Im, J.; He, S.; Chung, Y. Fiber-optic acetylene gas sensor based on microstructured optical fiber bragg gratings. *IEEE Photonic Technol. Lett.* **2011**, *23*, 1588–1590. [CrossRef]

9. Zhou, Q.; Liu, H.; Hong, C.; Xu, L.; Chen, W. Fabrication and enhanced acetylene sensing properties of PdO-decorated SnO_2 composites chemical sensor. *Sens. Lett.* **2016**, *14*, 1144–1149. [CrossRef]

10. Li, C.L.; Su, Y.; Lv, X.Y.; Xia, H.L.; Wang, Y.J. Electrochemical acetylene sensor based on Au/MWCNTs. *Sens. Actuators B Chem.* **2010**, *149*, 427–431. [CrossRef]

11. Zhou, Q.; Cao, M.; Li, W.; Tang, C.; Zhu, S. Research on acetylene sensing properties and mechanism of SnO_2 based chemical gas sensor decorated with Sm_2O_3. *J. Nanosci. Nanotechnol.* **2015**, *2015*, 714072.

12. Uddin, A.S.M.I.; Yaqoob, U.; Phan, D.-T.; Chung, G.-S. A novel flexible acetylene gas sensor based on PI/PTFE-supported Ag-loaded vertical ZnO nanorods array. *Sens. Actuators B Chem.* **2016**, *222*, 536–543. [CrossRef]

13. Lee, K.-W.; Phan, D.-T.; Chung, G.-S. Fabrication of low-temperature acetylene gas sensor based on Ag nanoparticles loaded hierarchical ZnO nanostructures. *Electron. Lett.* **2015**, *51*, 572–574. [CrossRef]

14. Uddin, A.S.M.I.; Phan, D.-T.; Chung, G.-S. Low temperature acetylene gas sensor based on Ag nanoparticles-loaded ZnO-reduced graphene oxide hybrid. *Sens. Actuators B Chem.* **2015**, *207*, 362–369. [CrossRef]

15. Lin, Y.; Li, C.; Wei, W.; Li, Y.; Wen, S.; Sun, D.; Chen, Y.; Ruan, S. A new type of acetylene gas sensor based on a hollow heterostructure. *RSC Adv.* **2015**, *5*, 61521–61527. [CrossRef]

16. Akash, K.; Sun-Woo, C.; Hyoun, W.K.; Sang, S.K. Highly sensitive and selective H_2 sensing by ZnO nanofibers and the underlying sensing mechanism. *J. Hazard. Mater.* **2015**, *286*, 229–235.

17. Rawal, I. Facial synthesis of hexagonal metal oxide nanoparticles for low temperature ammonia gas sensing applications. *RSC Adv.* **2015**, *5*, 4135–4142. [CrossRef]

18. Miller, D.R.; Akbar, S.A.; Morris, P.A. Nanoscale metal oxide-based heterojunctions for gas sensing: A review. *Sens. Actuators B Chem.* **2014**, *204*, 250–272. [CrossRef]

19. Shim, Y.S.; Kim, D.H.; Jeong, H.Y.; Kim, Y.H.; Nahm, S.H.; Kang, C.Y.; Kim, J.S.; Lee, W.; Jang, H.W. Utilization of both-side metal decoration in close-packed SnO_2 nanodome arrays for ultrasensitive gas sensing. *Sens. Actuators B Chem.* **2015**, *213*, 314–321. [CrossRef]

20. Zhang, Z.J.; Kaneti, Y.V.; Jiang, X.C.; Yu, A.B. Hydrothermal synthesis of sodium vanadium oxide nanorods for gas sensing application. *Sens. Actuators B Chem.* **2014**, *202*, 803–809. [CrossRef]

21. Zhang, L.; Zhao, J.; Zheng, J.; Li, L.; Zhu, Z. Hydrothermal synthesis of hierarchical nanoparticle-decorated ZnO microdisks and the structure-enhanced acetylene sensing properties at high temperatures. *Sens. Actuators B Chem.* **2014**, *158*, 144–150. [CrossRef]

22. Tamaekong, N.; Liewhiran, C.; Wisitsoraat, A.; Phanichphant, S. Acetylene sensor based on Pt/ZnO thick films as prepared by flame spray pyrolysis. *Sens. Actuators B Chem.* **2011**, *152*, 155–161. [CrossRef]

23. Chen, W.; Zhou, Q.; Gao, T.; Su, X.; Wan, F. Pd-doped SnO_2-based sensor detecting characteristic fault hydrocarbon gases in transformer oil. *J. Nanomater.* **2013**, *2013*, 127345. [CrossRef]

24. Uddin, A.S.M.I.; Lee, K.-W.; Chung, G.-S. Acetylene gas sensing properties of an Ag-loaded hierarchical ZnO nanostructure-decorated reduced graphene oxide hybrid. *Sens. Actuators B Chem.* **2015**, *216*, 33–40. [CrossRef]

25. Zhang, D.; Liu, J.; Xia, B. Quantitative detection of formaldehyde and ammonia gas via metal oxide-modified graphene-based sensor array combining with neural network model. *Sens. Actuators B Chem.* **2017**, *240*, 55–65. [CrossRef]

26. Alzari, V.; Sanna, V.; Biccai, S.; Caruso, T.; Politano, A.; Scaramuzza, N.; Sechi, M.; Nuvoli, D.; Sanna, R.; Mariani, A. Tailoring the physical properties of nanocomposite films by the insertion of graphene and other nanoparticles. *Compos. Part B Eng.* **2014**, *60*, 29–35. [CrossRef]

27. Gugliuzza, A.; Politano, A.; Drioli, E. The advent of graphene and other two-dimensional materials in membrane science and technology. *Curr. Opin. Chem. Eng.* **2017**, *16*, 78–85. [CrossRef]

28. Uddin, A.S.M.I.; Chung, G.-S. Synthesis of highly dispersed ZnO nanoparticles on graphene surface and their acetylene sensing properties. *Sens. Actuators B Chem.* **2014**, *205*, 338–344. [CrossRef]

29. Zhang, D.; Yin, N.; Xia, B. Facile fabrication of ZnO nanocrystalline-modified graphene hybrid nanocomposite toward methane gas sensing application. *J. Mater. Sci.-Mater. Electron.* **2015**, *26*, 5937–5945. [CrossRef]

30. Zhang, D.; Jiang, C.; Liu, J.; Cao, Y. Carbon monoxide gas sensing at room temperature using copper oxide-decorated graphene hybrid nanocomposite prepared by layer-by-layer self-assembly. *Sens. Actuators B Chem.* **2017**, *247*, 875–882. [CrossRef]

31. Zhang, D.; Liu, J.; Jiang, C.; Li, P.; Sun, Y. High-performance sulfur dioxide sensing properties of layer-by-layer self-assembled titania-modified graphene hybrid nanocomposite. *Sens. Actuators B Chem.* **2017**, *245*, 560–567. [CrossRef]

32. Bai, S.L.; Liu, J.C.; Guo, J.; Luo, R.X.; Li, D.Q.; Song, Y.J.; Liu, C.C.; Chen, A.F. Facile preparation of SnO_2/NiO composites and enhancement of sensing performance to NO_2. *Sens. Actuators B Chem.* **2017**, *249*, 22–29.

33. Ding, C.; Ma, Y.; Lai, X.; Yang, Q.; Xue, P.; Hu, F.; Geng, W. Mesoporous Ag/In_2O_3 composite derived from indium organic framework as high performance formaldehyde sensor. *J. Solid State Chem.* **2017**, *251*, 170–175.

34. Zhang, D.; Liu, J.; Xia, B. Nitrogen dioxide-sensing properties at room temperature of metal oxide-modified graphene composite via one-step hydrothermal method. *J. Electron. Mater.* **2016**, *45*, 4324–4330. [CrossRef]

35. Zhang, D.; Liu, J.; Chang, H.; Liu, A.; Xia, B. Characterization of a hybrid composite of SnO_2 nanocrystal-decorated reduced graphene oxide for ppm-level ethanol gas sensing application. *RSC Adv.* **2015**, *5*, 18666–18672. [CrossRef]

36. Zhang, D.; Chang, H.; Li, P.; Liu, R.; Xue, Q. Fabrication and characterization of an ultra-sensitive humidity sensor based on metal oxide/graphene hybrid nanocomposite. *Sens. Actuators B Chem.* **2016**, *225*, 233–240. [CrossRef]

37. Wang, X.; Zhao, M.; Liu, F.; Jia, J.; Li, X.; Cao, L. C_2H_2 gas sensor based on Ni-doped ZnO electrospun nanofibers. *Ceram. Int.* **2013**, *39*, 2883–2887. [CrossRef]

38. Liewhiran, C.; Tamaekong, N.; Wisitsoraat, A.; Phanichphant, S. Highly selective environmental sensors based on flame-spray-made SnO_2 nanoparticles. *Sens. Actuators B Chem.* **2012**, *163*, 51–60. [CrossRef]

39. Qi, Q.; Zhang, T.; Zheng, X.; Fan, H.; Liu, L.; Wang, R.; Zeng, Y. Electrical response of Sm_2O_3-doped SnO_2 to C_2H_2 and effect of humidity interference. *Sens. Actuators B Chem.* **2008**, *134*, 36–42. [CrossRef]

40. Zhang, D.; Sun, Y.; Jiang, C.; Zhang, Y. Room temperature hydrogen gas sensor based on palladium decorated tin oxide/molybdenum disulfide ternary hybrid via hydrothermal route. *Sens. Actuators B* **2017**, *242*, 15–24. [CrossRef]

41. Yang, H.; Li, J.; Yu, D.; Li, L. Seed/catalyst free growth and self-powered photoresponse of vertically aligned ZnO nanorods on reduced graphene oxide nanosheets. *Cryst. Growth Des.* **2016**, *16*, 4831–4838. [CrossRef]

42. Di Bartolomeo, A. Graphene schottky diodes: An experimental review of the rectifying graphene/semiconductor heterojunction. *Phys. Rep.* **2016**, *606*, 1–58. [CrossRef]

43. Kwon, Y.; Kim, H.; Lee, S.; Chin, I.J.; Seong, T.Y.; Lee, W.I.; Lee, C. Enhanced ethanol sensing properties of TiO_2 nanotube sensors. *Sens. Actuators B Chem.* **2012**, *173*, 441–446. [CrossRef]

44. Zhang, D.; Sun, Y.; Jiang, C.; Yao, Y.; Wang, D.; Zhang, Y. Room-temperature highly sensitive CO gas sensor based on Ag-loaded zinc oxide/molybdenum disulfide ternary nanocomposite and its sensing properties. *Sens. Actuators B Chem.* **2017**, *253*, 1120–1128. [CrossRef]